Solar-powered multi-scale sensor node on Imote2 platform for hybrid SHM in cable-stayed bridge

Duc-Duy Ho[1], Po-Young Lee[1], Khac-Duy Nguyen[1], Dong-Soo Hong[1], So-Young Lee[1],
Jeong-Tae Kim*[1], Sung-Woo Shin[2], Chung-Bang Yun[3] and Masanobu Shinozuka[4]

[1]Department of Ocean Eng., Pukyong National University, Busan, Korea
[2]Department of Safety Eng., Pukyong National University, Busan, Korea
[3]Department of Civil and Environmental Eng., KAIST, Daejeon, Korea
[4]Department of Civil and Environmental Eng., Univ. of California, Irvine, USA

Abstract.   In this paper, solar-powered, multi-scale, vibration-impedance sensor node on Imote2 platform is presented for hybrid structural health monitoring (SHM) in cable-stayed bridge. In order to achieve the objective, the following approaches are proposed. Firstly, vibration- and impedance-based hybrid SHM methods are briefly described. Secondly, the multi-scale vibration and impedance sensor node on Imote2-platform is presented on the design of hardware components and embedded software for vibration- and impedance-based SHM. In this approach, a solar-powered energy harvesting is implemented for autonomous operation of the smart sensor nodes. Finally, the feasibility and practicality of the smart sensor-based SHM system is evaluated on a full-scale cable-stayed bridge, Hwamyung Bridge in Korea. Successful level of wireless communication and solar-power supply for smart sensor nodes are verified. Also, vibration and impedance responses measured from the target bridge which experiences various weather conditions are examined for the robust long-term monitoring capability of the smart sensor system.

Keywords: solar power; vibration; impedance; Imote2; hybrid; SHM; cable-stayed bridge.

1. Introduction

Recent tragic collapses of bridges and buildings have awoken public on the need of structural health monitoring (SHM) that can play an important role in the safety and service life of civil infrastructures. In order to secure the structural integrity, many robust sensing technologies and SHM methods have been developed (Doebling *et al.* 1998, Sohn *et al.* 2003, Koo 2008, Kim *et al.* 2010). The SHM techniques are usually classified as two groups: global and local SHM methods. Global SHM methods mostly use structural responses representing the behavior of entire structure. For example, low frequency responses such as acceleration, natural frequency and mode shape are used to examine structural damage in global level (Adams *et al.* 1978, Stubbs and Kim 1996, Kim *et al.* 2006). However, these methods are less sensitive to local damage. On the other hand, local SHM methods mainly deal with local critical members by using high frequency structural responses. For example, high frequency responses of electro-mechanical impedance or guided wave are used to monitor damage in local zones, but with limited sensing ranges (Sun *et al.* 1995, Liang *et al.* 1996,

---

Park *et al.* 1999, Park *et al.* 2003, Raghavan and Cesnik 2007). As a result, there is a need to combine global and local SHM methods for the sake of efficiency as well as accuracy in SHM for complex-type structures, which have a variety of member types and many critical joints.

Kim *et al.* (2010) proposed a hybrid SHM methodology combining vibration- and impedance-based methods to pursue damage monitoring and estimation in global structural level and, at the same time, in local critical members of prestressed concrete girder bridges. Their approaches include the followings. First, a global occurrence of damage was alerted by monitoring change in acceleration features. Next, the alerted damage is classified into either local or global damage by using the change in impedance signatures. Then, the location and extent of damage are estimated using changes in vibration modal parameters.

The commercial SHM system mainly requires a number of sensors, a huge amount of signal transmitting wires, data acquisition instruments and centralized data storage servers. Therefore, the cost associated with installation and maintenance of SHM system is very high. For example, Tsing Ma suspension bridge in Hong Kong was installed more than 350 wired sensors for SHM purpose. The total cost associated with installation of bridge monitoring system was over US$8 million (Farrar 2001). The installation of cables for wired SHM system was up to 25% of the total system cost and 75% of the installation time (Straser and Kiremidjian 1998). Recently, low-cost, stand-alone, smart sensors have been developed for SHM by many research groups. Straser and Kiremidjian (1998) first proposed a design of a low-cost wireless modular monitoring system for SHM applications. Since then, many researchers have developed wireless sensors based on a variety of sensor platforms (Spencer *et al.* 2004, Lynch *et al.* 2006, Mascarenas *et al.* 2007, Nagayama *et al.* 2009, Rice *et al.* 2010, Kim *et al.* 2011, Spencer and Cho 2011). By adopting those smart sensors for SHM in large structures, the costs are greatly reduced and the data processing and information management will be very effective by ways of sensing and on-board computation, wireless transmission, and green energy harvesting.

The previous works have been mainly focused on implementing single-scale wireless sensor node for SHM on lab-scale structures. There have been a few full-scale implementations of wireless sensors for bridge monitoring so far (Jang *et al.* 2010, Cho *et al.* 2010, Spencer and Cho 2011). Additionally, solar energy harvesting system has been adopted to extend the lifetime of smart sensors, especially, for long-term monitoring applications. For field SHM applications, the use of batteries for powering to sensor nodes has a disadvantage since it is inconvenient to regularly replace low-capacity batteries located within complex structural geometries. On cable-stayed bridges, for example, sensor nodes installed on cables and top pylons are difficult for replacing batteries. Hence, solar power is one of the best ways to supply electricity for autonomous smart sensor nodes.

In this paper, solar-powered, multi-scale, vibration-impedance sensor node on Imote2 platform is presented for hybrid SHM of a full-scale cable-stayed bridge. Firstly, vibration- and impedance-based hybrid SHM methods employed in this study are briefly described. Secondly, the multi-scale vibration-impedance sensor node is presented on the design of hardware components and embedded software for vibration- and impedance-based SHM. In this approach, a solar-powered energy harvesting is implemented for autonomous operation of smart sensor nodes. Finally, the feasibility of the smart sensor-based SHM system is evaluated on Hwamyung cable-stayed bridge, in Korea. Successful level of wireless communication and solar-power supply for smart sensor nodes are verified. Also, vibration and impedance responses measured from the target bridge which experiences various weather conditions (e.g., typhoon Meari) are examined for the robust long-term monitoring capability of the smart sensor system.

2. Vibration and impedance-based SHM methods

2.1 Vibration-based SHM Methods

Vibration-based SHM methods utilize various dynamic features extracted from measured acceleration signals. Vibration-based SHM is performed in four steps: (1) to measure vibration signals for distributed locations of sensors; (2) to extract vibration features (i.e., power spectral density, natural frequency and mode shape) for entire structure by using modal identification methods such as frequency domain decomposition (FDD) method or stochastic subspace identification (SSI) method (Brincker *et al.* 2001, Yi and Yun 2004); (3) to identify damage occurrence in entire structure by performing change in natural frequency, correlation coefficient of power spectral densities (Kim *et al.* 2010); and (4) to estimate the location and severity of damage, for example, the change in cable force (Zui *et al.* 1996). We selected three methods as follows:

Firstly, the relative change in natural frequency is selected for global damage monitoring since the natural frequency is a global property of structure. The relative change in the ith natural frequency before and after the occurrence of structural damage is determined as

$$\frac{\delta f_i}{f_i} = \frac{f_i^* - f_i}{f_i} \times 100\%$$ (1)

where f_i, f_i^* are the ith natural frequency before and after damage, respectively.

Secondly, the correlation coefficient (CC) of power spectral densities (PSDs) obtained before and after the occurrence of damage is calculated by the following equation (Kim *et al.* 2010).

$$\rho_{XY} = \frac{E[S_{xx}(f)S_{yy}(f)] - E[S_{xx}(f)]E[S_{yy}(f)]}{\sigma_{S_{xx}} \sigma_{S_{yy}}}$$ (2)

where $E[\cdot]$ is the expectation operator; $S_{xx}(f)$ and $S_{yy}(f)$ are the PSDs of two time signals before and after damage, respectively; and $\sigma_{S_{xx}}$, $\sigma_{S_{yy}}$ are the corresponding standard deviations of PSDs, respectively.

Thirdly, during the last decades, several methods have been proposed for estimation of cable force using natural frequency (Shimada 1995, Zui *et al.* 1996). Among those, the method proposed by Zui *et al.* (1996) considers effects of both flexural rigidity and cable-sag on cable force estimation. Based on the concept of the method, the following practical formula using multiple modes is used for estimation of cable force.

$$T = \frac{1}{NM} \sum_{n=1}^{NM} T_n$$ (3)

where T is the average tension force; NM is the number of vibration mode; and T_n is the tension force using the nth mode and is determined as follow (Zui *et al.* 1996)

$$T_n = \frac{4m}{n^2}(f_n L)^2 \left[1 - 2.2n\frac{C}{f_n} - 0.55n\left(\frac{C}{f_n}\right)^2\right]; \quad \xi < 200$$ (4)

$$T_n = \frac{4m}{n^2}(f_n L)^2 \left[1 - 2.2n\frac{C}{f_n}\right]; \quad \xi \geq 200$$ (5)

where ξ is the parameter determined from cable properties and design conditions, $\xi = \sqrt{(T/EI)} \times L$; EI is the flexural rigidity of cable; L is the span length of cable; m is the mass of cable per unit length; f_n is the natural frequency corresponding to the nth mode; and $C = \sqrt{(EI/mL^4)}$.

2.2 Impedance-based SHM methods

Mechanical impedance of host structure is a function of mass, damping and stiffness. When a structure is damaged, its mechanical impedance would be changed. Any changes in dynamic characteristics of host structure, hence, can be represented by the change in impedance signatures (Sun *et al.* 1995, Liang *et al.* 1996, Park *et al.* 2003, Kim *et al.* 2010). The impedance-based SHM is performed in four steps: (1) to measure impedance signal from PZT sensor bonded to local critical member; (2) to extract impedance features such as real part, imaginary part, phase and magnitude; (3) to monitor the damage occurrence in local member by using statistical index based methods such as root mean square deviation of impedance signatures; and (4) to identify the pattern of damage.

In order to quantify the change in impedance signatures due to structural damage, the root mean square deviation (RMSD) of impedance signatures is utilized. The RMSD is calculated from impedance signatures measured before and after damage as (Sun *et al.* 1995)

$$RMSD(Z, Z^*) = \sqrt{\sum_{i=1}^{N} [Z^*(\omega_i) - Z(\omega_i)]^2 / \sum_{i=1}^{N} [Z(\omega_i)]^2} \qquad (6)$$

where $Z(\omega_i)$ and $Z^*(\omega_i)$ are the impedances measured before and after damage for the ith frequency, respectively; and N denotes the number of frequency points in the sweep.

3. Solar-powered multi-scale vibration-impedance sensor node

3.1 Hardware design of smart sensor nodes

For the vibration- and impedance-based hybrid SHM, a solar-powered multi-scale vibration-impedance sensor node on Imote2 platform is designed as schematized in Fig. 1. The high-performance sensor platform, Imote2, provided by Memsic Co. (2010) was selected to control the operation of the sensor node. For vibration monitoring, SHM-A and SHM-H sensor boards developed by University of Illinois at Urbana-Champaign (UIUC) (Rice *et al.* 2010, Jo *et al.* 2010) were selected. For impedance monitoring, an Imote2-platformed impedance sensor board (SSeL-I) developed by Pukyong National University (PKNU) (Kim *et al.* 2011) was selected. As also shown in Fig. 1, the solar-powered energy harvesting is designed by employing solar panel and rechargeable battery.

The Imote2 platform was built with 13~416 MHz PXA271 XScale processor (Crossbow Technology 2007). This processor integrates 256 kB SRAM, 32 MB flash memory and 32 MB SDRAM. It also integrates many I/O options such as 3×UART, I2C, 2×SPI, SDIO, I2S, AC97, USB host, Camera I/F, GPIO. Therefore, Imote2 platform is very flexible in supporting different sensor types, ADC chips and radio options. A 2.4 GHz surface mount antenna which has a communication range of about 30 m is equipped for each Imote2 platform. In addition, an SMA connector is soldered directly to the board for connecting to external antenna in case of longer communication range is desired. The Imote2 platform connects with sensor boards and battery board by basic connectors.
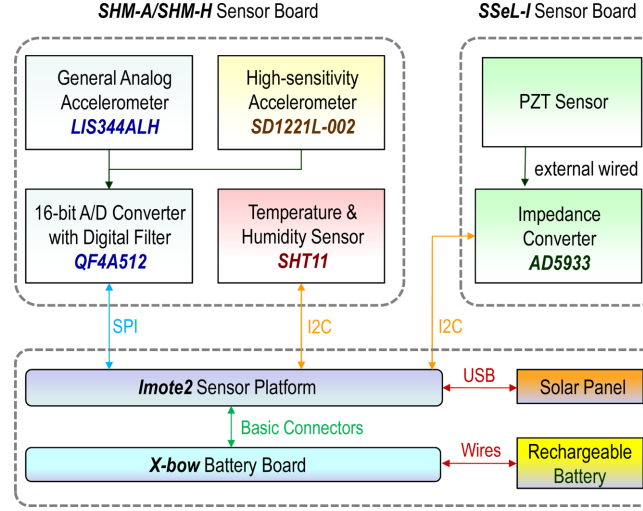
Fig. 1 Design of solar-powered multi-scale vibration-impedance sensor node

The SHM-A and SHM-H sensor boards include several key components such as accelerometer, anti-aliasing filter and analog-to-digital converter (ADC). The SHM-A sensor board employs tri-axial LIS344ALH accelerometer which has input range ± 2 g, sensitivity 0.66 V/g and output noise 50 μg/$\sqrt{\text{Hz}}$. Meanwhile, the SHM-H sensor board employs SD1221L-002 accelerometer for high-sensitivity channel which has input range ± 2g, sensitivity 2 V/g and output noise 5 μg/$\sqrt{\text{Hz}}$. These sensor boards, additionally, have TAOS2561 light-to-digital sensor, Sensirion SHT11 digital relative humidity and temperature sensor. Also, the 4-channel 16-bit high resolution ADC with digital anti-aliasing filters (QF4A512) is adopted. By adopting the programmable digital filters, the sensor board provides user-selectable sampling rates and cut-off frequencies that can meet a wide range of applications for civil infrastructure monitoring.

The SSeL-I sensor board was designed on the basis of original impedance sensor nodes presented by Mascarenas *et al.* (2007) and Park *et al.* (2010). The sensor board consists of an impedance converter AD5933, two pull-up resistors for I2C communication, two capacitors for bypassing noises, a connector to PZT patches and two connectors to the Imote2 sensor platform. The AD5933 impedance converter has the following embedded multi-functional circuits: function generator, digital-to-analog converter, current-to-voltage amplifier, anti-aliasing filter, ADC, and discrete Fourier transform (DFT) analyzer. With measurable range from 1 kHz to 100 kHz (Analog Devices 2010), this chip converts real and imaginary of impedance signatures at a target frequency and transmits these values into the microcontroller.

In order to deal with power supply issue, especially for long-term operation of smart sensor nodes, energy harvesting is essential. Among natural power sources, solar power is a valuable selection for Imote2 platform. Optionally, the Imote2 can be powered by primary battery, rechargeable battery or USB power. For powering by rechargeable battery, the hardware of X-bow battery board must be modified. More detail about the hardware modifications can be found in Miller *et al.* (2010). Due to the requirement for solar panel integrated with Imote2 such as output voltage range 4.6~10 V and output current range 115~1400 mA, SPE-350-6 solar panel (9 V, 350 mA) provided by SolarMade is a suitable selection. In addition, Powerizer Li-ion polymer rechargeable battery
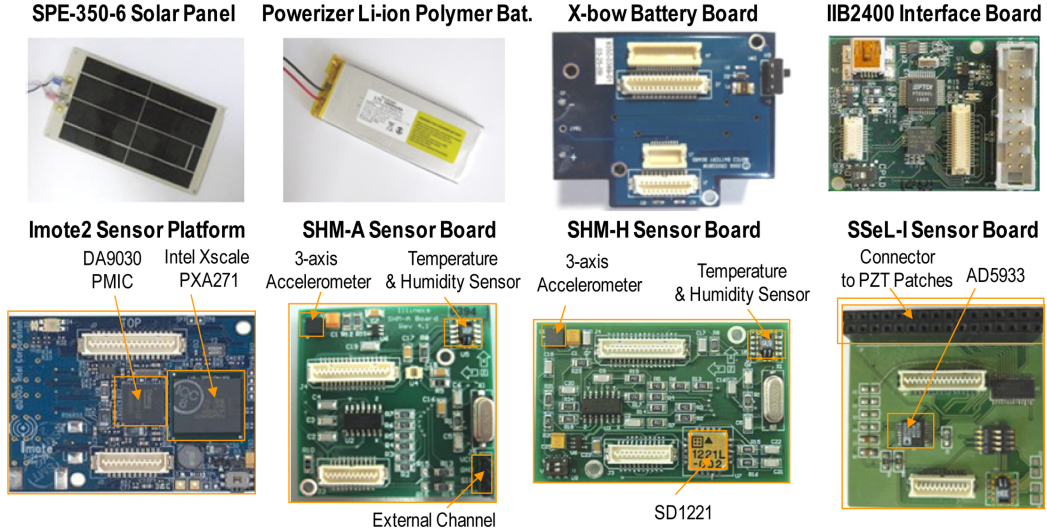
Fig. 2 Hardware components for solar-powered multi-scale vibration-impedance sensor node

which has the capacity of 10000 mAh, normal voltage of 3.7 V which can be charged up to 4.2 V, and contains a protection circuit is also employed. Fig. 2 shows hardware components required for solar-powered multi-scale vibration-impedance sensor node.

3.2 Embedded software for smart sensor nodes

As schematized in Fig. 3, device drivers for smart sensor nodes 'Imote2/SHM-A/SHM-H/SSeL-I' are programmed according to UIUC ISHMP Service Toolsuite and PKNU SSeL SHM Tools (Park *et al.* 2010). For synchronized acceleration measurements, *RemoteSensing* component from ISHMP Services Toolsuite is used for the SHM-A/SHM-H sensor boards. After all leaf nodes located on a structure finish acceleration measurements, each leaf node transmits the measured data to a gateway node. Then the data is processed to feature extraction and damage detection programmed in SSeL SHM Tools. For the SHM-A/SHM-H sensor boards, the SSeL SHM tools include a device driver for ADC and mathematical functions for damage monitoring such as PSD, CC of PSDs. Also, the FDD and SSI methods are embedded into the system to extract modal parameters such as natural frequencies and mode shapes.

For the impedance measurements from the SSeL-I sensor board, *I2CControl* component provided from ISHMP Services Toolsuite and *Impedance* component (i.e., the device driver to operate AD5933) programmed in SSeL SHM Tools are utilized. First, each leaf node measures impedance signals and transmits the measured data to the gateway node. Then the gateway node performs the impedance-based damage detection. For the SSeL-I impedance sensor board, the SSeL SHM Tools include a device driver for impedance measurement and mathematical functions for damage monitoring such as CC, RMSD of impedance signatures.

For charging the battery, *ChargeControl* component from ISHMP Services Toolsuite is employed. This component is developed to check battery voltage and to control charging process. If the battery voltage is less than 3.9 V or the charging voltage is adequate (more than 4.1 V), the charging mode will be initiated. If the battery voltage is sufficient, the Imote2 goes to sleep mode. The *ChargeControl*
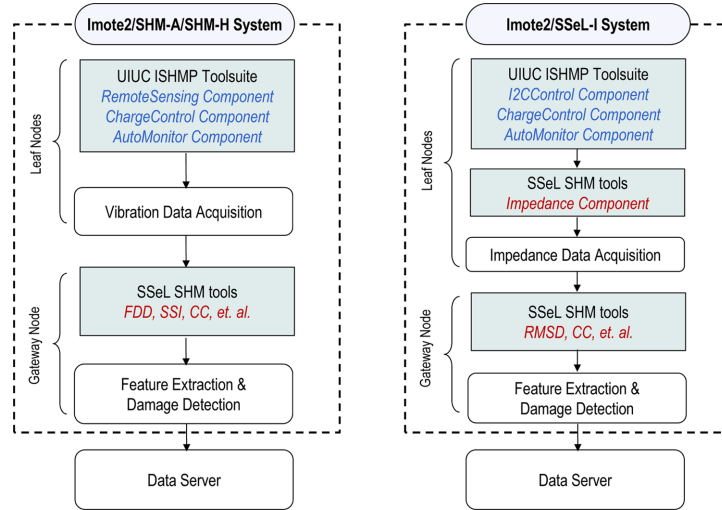
Fig. 3 Embedded software for solar-powered multi-scale vibration-impedance sensor node

component works in conjunction with *SnoozeAlarm* component (Miller *et al.* 2010) which frequently check charging voltage and battery voltage for the efficient charging process.

AutoMonitor is another advanced component of ISHMP Service Toolsuite that allows autonomous operation of sensor network by combining three components: *ThresholdSentry*, *RemoteSensing* and *AutoUtilCommand*. *ThresholdSentry* is a component that periodically wakes leaf nodes at pre-defined time to measure data with *RemoteSensing* component. *AutoUtilCommand* is a component that reads and sends the values of supply voltage, temperature and charging status to the gateway node. The interval time to execute *AutoMonitor* component is defined by user. More detail about the operation of *AutoMonitor* component can be found in "Imote2 for Structural Health Monitoring: User's Guide" (Illinois Structural Health Monitoring Project 2011).

4. Field evaluation of smart sensor nodes on Hwamyung bridge

4.1 Experiments on Hwamyung bridge

In this study, the hardware and software developed for the smart sensor nodes are evaluated on Hwamyung cable-stayed bridge in Korea. This field deployment is a collaborative research between Korea (Pukyong National University and KAIST) and USA (University of California, Irvine). The main purpose of this deployment is to demonstrate the feasibility and practicality of the smart sensor nodes for full-scale SHM applications.

4.1.1 Description of Hwamyung bridge

Hwamyung Bridge is a cable-stayed bridge crossing Nakdong river between Busan and Gimhae, Korea, as shown in Fig. 4. The bridge has been constructed by Hyundai Engineering & Construction Co., Ltd., from December 2004 to June 2011. It is the longest cable-stayed bridge with prestressed concrete box girder in Korea as so far. The geometry of the bridge is designed

(a) Bridge location

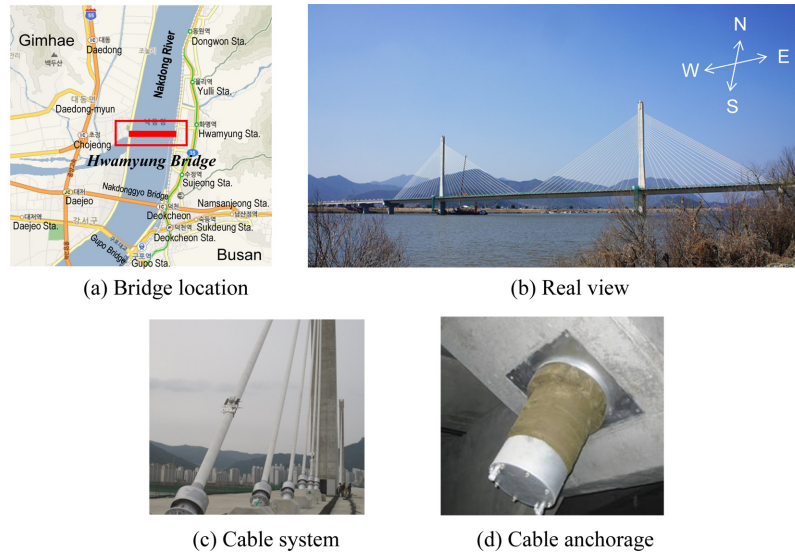
(b) Real view

(c) Cable system

(d) Cable anchorage

Fig. 4 On-site view of Hwamyung cable-stayed bridge

as detailed in Fig. 5. As shown in Fig. 5(a), the bridge consists of three spans including a 270 m central main span between two pylons and two 115 m side spans connecting east and west approaches. The clearance of the deck is 14.7 m from the water level. The height of two pylons is 65 m from deck level. As shown in Fig. 5(b) the box girder supported by single plane stayed-cable is 27.8 m in width and 4 m in height. The bridge has total 72 cables, positioning 18 cables at one side of pylon. As listed in Table 1, there are six different cable groups (i.e., 49H, 55H, 61H, 73H, 75H, and 85H) dependent upon the number of strands. The cable groups are covered by high-density polyethylene (HDPE) ducts with different diameters as 200 mm, 225 mm, 250 mm, and 280 mm. Specifications of the six cable groups are detailed as listed in Table 1.
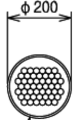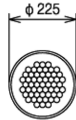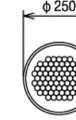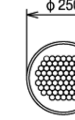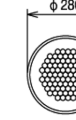
4.1.2 Field deployment of smart sensor nodes

In order to monitor the responses of Hwamyung cable-stayed bridge, two hardware configurations of Imote2-based smart sensor nodes which are gateway node and leaf node are designed. As schematized in Fig. 6, a gateway node consists of an Imote2 platform with 2.4 GHz antenna, an IBB2400 interface board connected to the PC via USB cable. A leaf node consists of an Imote2 platform with 2.4 GHz antenna, a sensor board (e.g., SHM-A, SHM-H, SSeL-I), X-bow battery board powered by D-cell battery or by Powerizer Li-ion polymer rechargeable battery with or without SPE-350-6 solar panel.

Fig. 6 shows the layout of field sensor deployment on Hwamyung cable-stayed bridge. For vibration measurement of the bridge, total sixteen (16) smart sensor nodes (Imote2/SHM-A/SHM-H) including fifteen leaf nodes and one gateway node (i.e., gateway acceleration) were installed. Four Imote2/SHM-H sensors were placed on four cables (i.e., C1, C2, C4, and C5). Six Imote2/SHM-H sensors were placed at five locations of the deck and at the top of the west pylon (i.e., D1, D2, D3, D4, D5, and P1). As also shown in Fig. 6, five Imote2/SHM-A sensors were placed on five selected cables (i.e., C1~C5). For each sensor board (i.e., SHM-H or SHM-A), three axes accelerations were measured in duration 600 seconds with sampling rate 25 Hz. Therefore, total 45 channels were used

for acceleration measurement in Hwamyung Bridge.

As also noted in Fig. 6, total six (6) smart sensor nodes (Imote2/SSeL-I) including one gateway node (i.e., gateway impedance) were installed for impedance measurement of cable system. Five leaf nodes were employed on the five selected cables (i.e., C1~C5). The impedance signatures were measured in frequency range of 10 kHz~100 kHz with 500 intervals of sweeping frequency. Note that the measured frequency range was the same as the capacity of the SSeL-I impedance sensor board as mentioned before (section 3.1).

All sensor nodes and base station are placed in plastic boxes which have waterproof rubber gaskets, as shown in Fig. 7, to prevent them from sun-heating, absorbent, and other damage caused by harsh environmental condition such as rain, wind, and dust at the field site. The base station includes a PC, two gateway nodes (one for acceleration measurement and another for impedance measurement) and a commercial broadband (T-login) modem to connect the PC to internet. Note that the two gateway nodes were set up with different USB ports and radio channels to avoid the interference in transmitting commands to and receiving data from leaf nodes. An external antenna was connected to Imote2 platform of each sensor node. Solar panels were mounted on the sensor boxes to harvest the solar energy for recharging the Li-ion polymer batteries embedded to the sensor boards. A webcam was installed on the west pylon to observe the bridge's condition in real-time.

(a) Side view

(b) Girder section

Fig. 5 Geometry of Hwamyung cable-stayed bridge

Table 1 Specifications of cables in Hwamyung cable-stayed bridge

Anchorage type	49H	55H	61H	73H	75H	85H
Strand Num.	49	55	61	73	75	85
Cable cross section	φ 200	φ 225	φ 225	φ 250	φ 250	φ 280
Nominal area (mm^2)	7350	8250	9150	10950	11250	12750
Moment of inertial (mm^4)	4.3×10^6	5.42×10^6	6.66×10^6	9.54×10^6	1.01×10^7	1.29×10^7
Tensile strength (kN)	13671	15345	17019	20367	30925	23715
Elastic modulus (GPa)	195	195	195	195	195	195
Unit mass (kg/m)	67.54	76.34	84.14	101.0	103.6	118.35
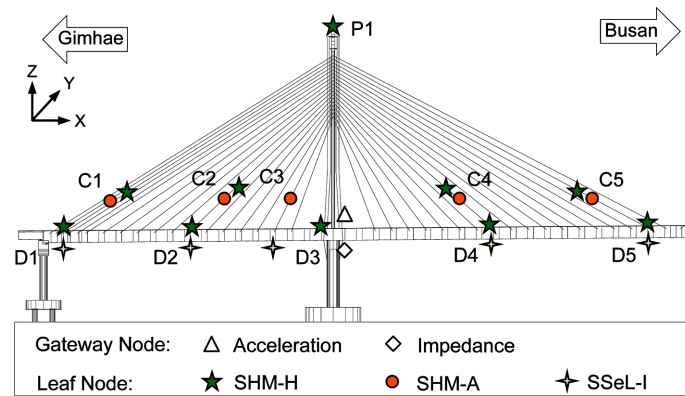
Fig. 6 Field sensor layout on Hwamyung Bridge: 45 Acceleration CHs and 5 Impedance CHs

(a) Deck node (b) Top pylon node (c) Cable node

(c) Gateway node and webcam (d) Impedance node (f) Gateway base station
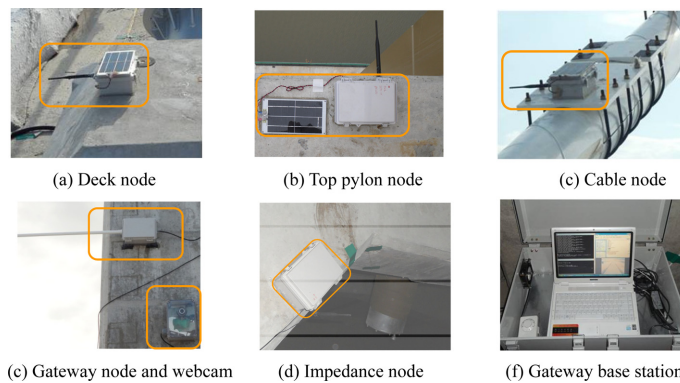
Fig. 7 Field deployment of smart sensor nodes on Hwamyung Bridge

4.2 Long-term monitoring performance of smart sensor nodes

4.2.1 Test history

The Hwamyung Bridge was monitored by the smart sensor nodes for three months (from 21st June to 20th September, 2011). The bridge was instrumented on two separate periods. In the first

period (from 21st June to 14th July, 2011), accelerations were only measured by the Imote2/SHM-A and Imote2/SHM-H. Note that a typhoon named Meari passed though the Korean peninsula on 25th and 26th June, 2011. In the second period (from 7th August to 20th September, 2011), accelerations and impedances were measured by the Imote2/SHM-A, Imote2/SHM-H, and Imote2/SSeL-I.

4.2.2 Wireless communication and power consumption

Responses of the bridge were measured by smart sensor nodes with *AutoMonitor* two-hour interval under ambient vibration condition. During the monitoring period, working status of the sensor system was evaluated. Fig. 8 shows performance evaluation of wireless communication from 25th June to 14th July, 2011. As indicated in the figure, the characters 'H' and 'A' denote the Imote2/SHM-H and Imote2/SHM-A, respectively. The sensor nodes were well responsive (i.e., 90% successful level), except the sensor nodes distanced far from base station (i.e., sensors D1, C1, C5). During sensing, the SHM-H sensor board consumes more power than the SHM-A sensor board. When the battery is low, the Imote2 sensor platform may not supply the required voltage for the SHM-H sensor board. As a result, the working status of the Imote2/SHM-A was better than that of the Imote2/SHM-H.

Fig. 9 shows performance evaluation of power consumption for three sensor nodes (i.e., sensors P1, D2, C4) during twenty days (i.e., 25th June~14th July, 2011) due to the change in weather conditions. The voltage of sensor node integrated with solar panel and rechargeable battery (i.e., sensor P1)
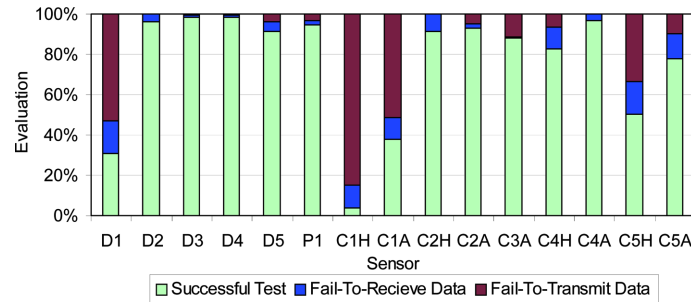

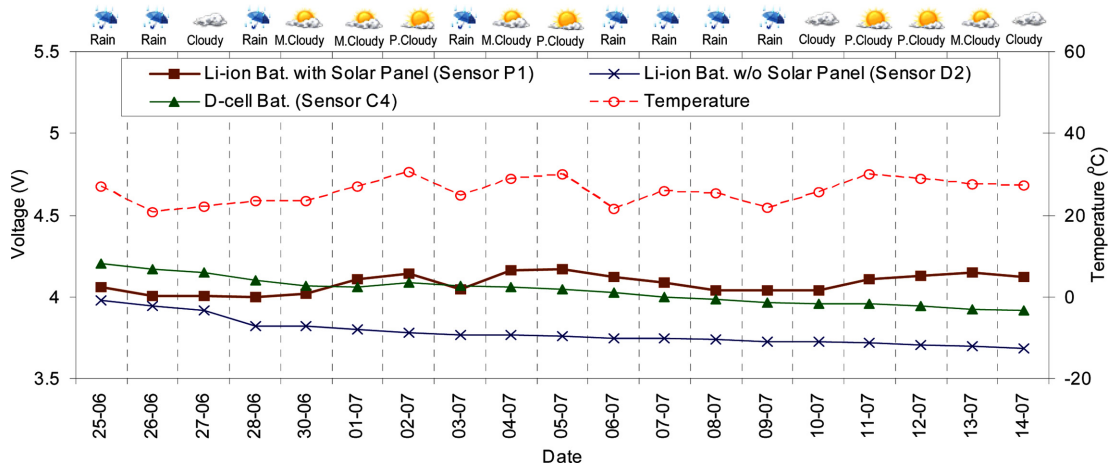Fig. 8 Performance evaluation of wireless communication

Fig. 9 Performance evaluation of power consumption

remained around 4.1 V. Meanwhile, the voltages of sensor nodes integrated with only rechargeable battery (i.e., sensor D2) or D-cell batteries (i.e., sensor C4) were decreased day after day. This proves that the charging process of solar-powered sensor nodes was stably working.

4.2.3 Vibration monitoring under typhoon condition

In this section, vibration responses of the bridge measured and analyzed due to the change in weather conditions are described. On 25th and 26th June, 2011, the typhoon Meari passed through the Korean peninsula and directly affected the site of Hwamyung Bridge. Figs. 10-12 show acceleration responses and PSDs measured from top pylon P1, deck D2 and cable C4 under normal condition and typhoon Meari, respectively. The natural frequencies indicated in the figures were determined by reading the peak frequencies in PSD functions. These peak frequencies were set up based on numerical natural frequencies which were determined from FE analysis for deck and pylon and string theory (Clough and Penzien 1993) for cables. During the typhoon period, the vibration of the bridge almost increased as much as 2 times for top pylon P1 (i.e., 0.6 mg to 1.1 mg), 3 times for deck D2 (i.e., 0.3 mg to 0.9 mg), and 2 times for cable C4 (i.e., 14 mg to 29 mg). The natural frequencies of top pylon P1 and deck D2 were remained unchanged during the typhoon pass, as shown in Figs. 10 and 11. Meanwhile, the natural frequencies of cable C4 were reduced about 0.2% for mode 2 and 0.3% for mode 3, as shown in Fig. 12. Note that there are unexpected periodical peaks (i.e., 0.8 Hz, 1.6 Hz) in frequency domain as shown in Fig. 11. Those indications are unexpected from numerical modal analysis, which is described in the later part. It has been reported that these noisy peaks can be caused by power supply issue of SHM-H sensor board (Jo *et al.* 2010). Further studies should be made to resolve the problem related to the performance of the SHM-H sensor board.

4.2.4 Long-term vibration and impedance monitoring under weather change

The performance of the smart sensor nodes was evaluated for vibration- and impedance-based monitoring under long-term ambient condition. The cable C3 was selected as a target structure. During five-day experiment (13th to 17th August, 2011), acceleration and impedance signatures were
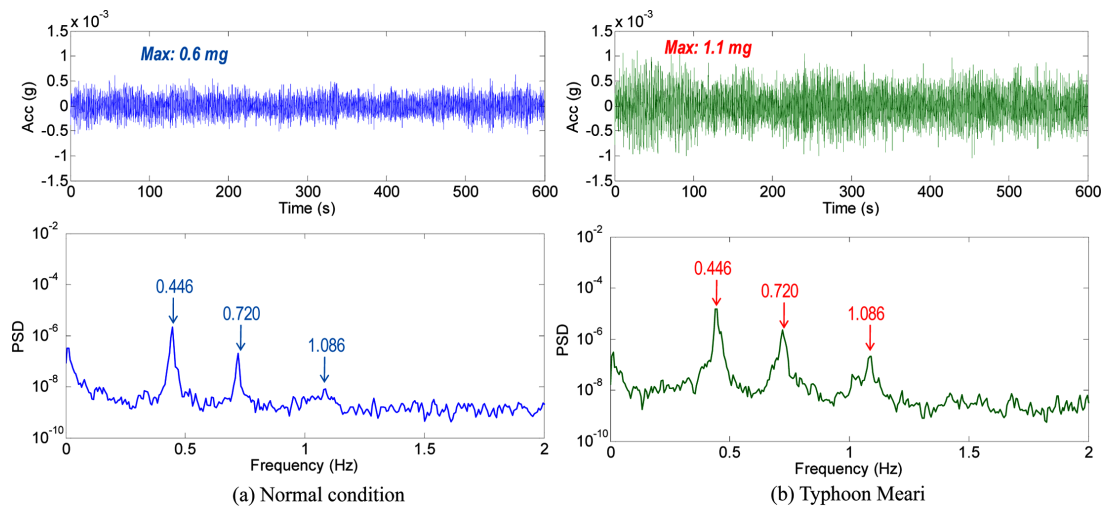

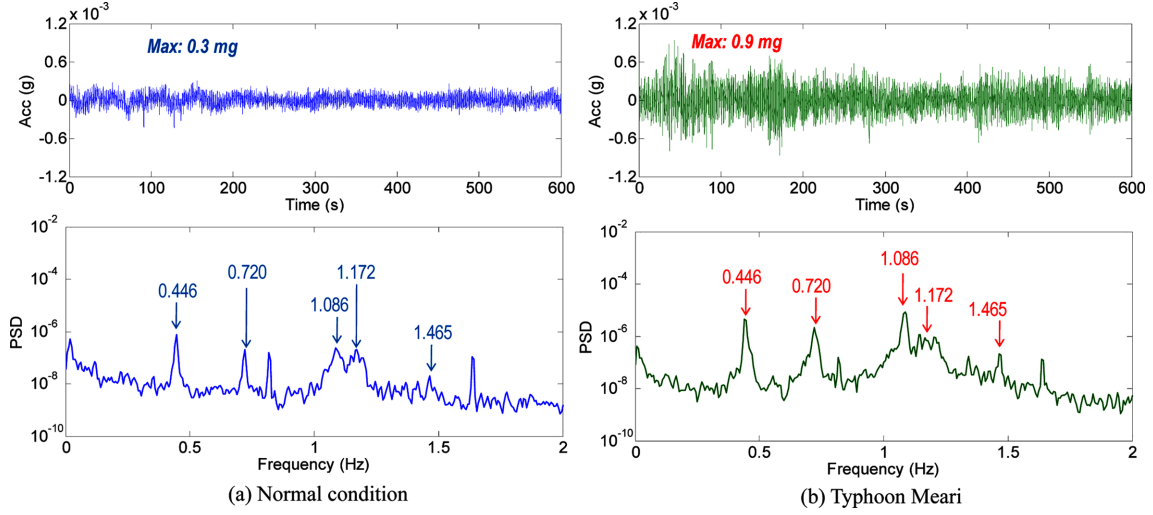Fig. 10 Acceleration responses and power spectral densities of top pylon P1

(a) Normal condition   (b) Typhoon Meari

Fig. 11 Acceleration responses and power spectral densities of deck D2

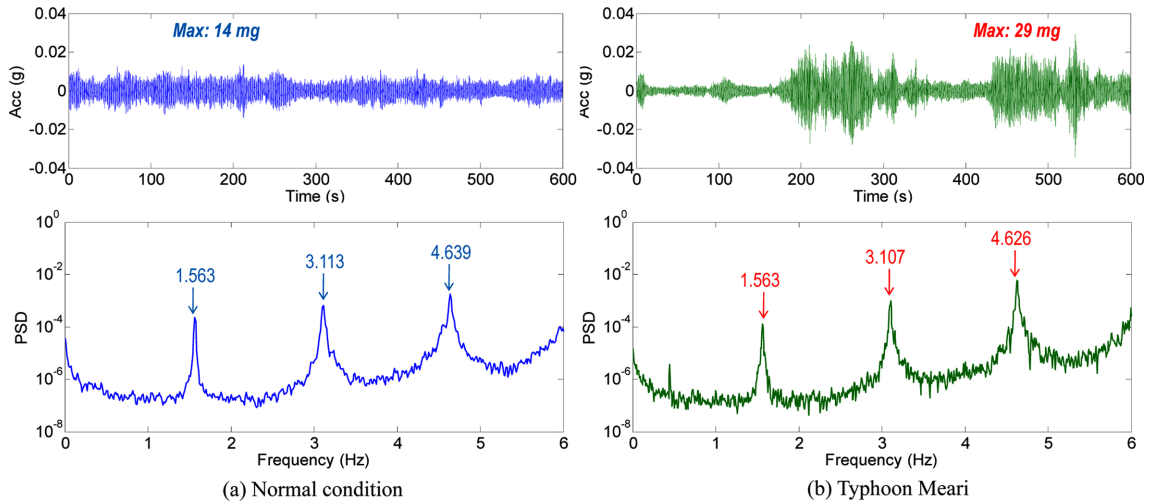(a) Normal condition   (b) Typhoon Meari

Fig. 12 Acceleration responses and power spectral densities of cable C4

recorded at the same time by the smart sensor nodes located on cable C3 which is indicated in Fig. 6. Fig. 13 shows vibration and impedance responses monitored during the period by the smart sensor nodes. It is observed from the figure when the temperature slightly goes up (i.e., 26°C to 30°C), the PSDs shift to left side indicating the cable's natural frequency reduction, meanwhile, the real impedance signatures shift to right side indicating the cable's impedance frequency increment.

Fig. 14 shows the vibration and impedance monitoring results versus the weather conditions for the five-day experiment. Fig. 14(a) shows relative changes in the first natural frequency versus the temperature change. It is noticed that the natural frequency is relatively sensitive to the temperature change. The natural frequency decrease as the temperature goes up, and vice versa. As shown in Fig. 14(b), the CC of PSDs consistently changes due to the change in weather conditions. From the

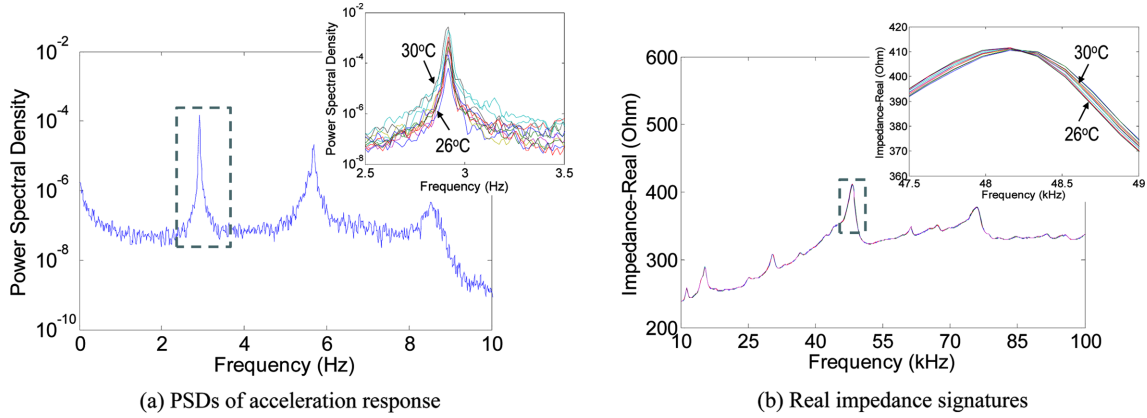(a) PSDs of acceleration response   (b) Real impedance signatures

Fig. 13 Vibration and impedance responses on cable C3

impedance monitoring results shown in Fig. 14(c), it is observed that the RMSD index consistently changes as the temperature repeatedly goes up and down. It is also noticed that the impedance signatures are more correlated to the temperature change than the natural frequencies and PSDs of acceleration signals. The multi-scale aspect of the sensor nodes was demonstrated by examining the same sets of vibration and impedance responses in the same period of time.

4.3 Cable force monitoring of test bridge

4.3.1 Vibration-based cable force monitoring

For cable-stayed bridge, cable force is one of the important targets needed to be monitored for the safety and service life of the bridge. In order to estimate cable force, cable's natural frequencies should be accurately measured. The SSI method (Yi and Yun 2004) was employed to extract the cable's natural frequencies. The SSI method gives more accurate natural frequency than reading the peak frequency in PSD function. Frequency ranges are set up based on theoretical natural frequencies which are calculated by string theory (Clough and Penzien 1993). Structural properties of the five selected cables (i.e., C1~C5) are given in Table 2. The theoretical natural frequencies of the cables are calculated for the first three cable modes with regarding to designed forces, as listed in Table 2.

From acceleration signals measured by Imote2/SHM-A sensor nodes on the five cables C1~C5, the first three natural frequencies were measured at temperature 27.9°C, as listed in Table 2. Those natural frequencies are very similar to the theoretical natural frequencies. That implies the existing forces in the five cables are very close to the designed ones. For more feasible comparison, cable forces of the five cables C1~C5 were estimated by using the frequency-based cable force model stated in Eqs. (3)-(5). In comparison with designed values, Fig. 15(a) shows the estimated cable forces for the cables C1~C5. The results show good agreement with small differences, as listed in Table 2. The differences varied within 0.4%~10.3% depending on the cables. The estimated forces which were calculated from the experimental data reflect the real value of cable forces more accurately than the designed forces which were determined from the design conditions. Note that the estimated forces depend on the number of vibration modes used for the frequency-based cable force model.
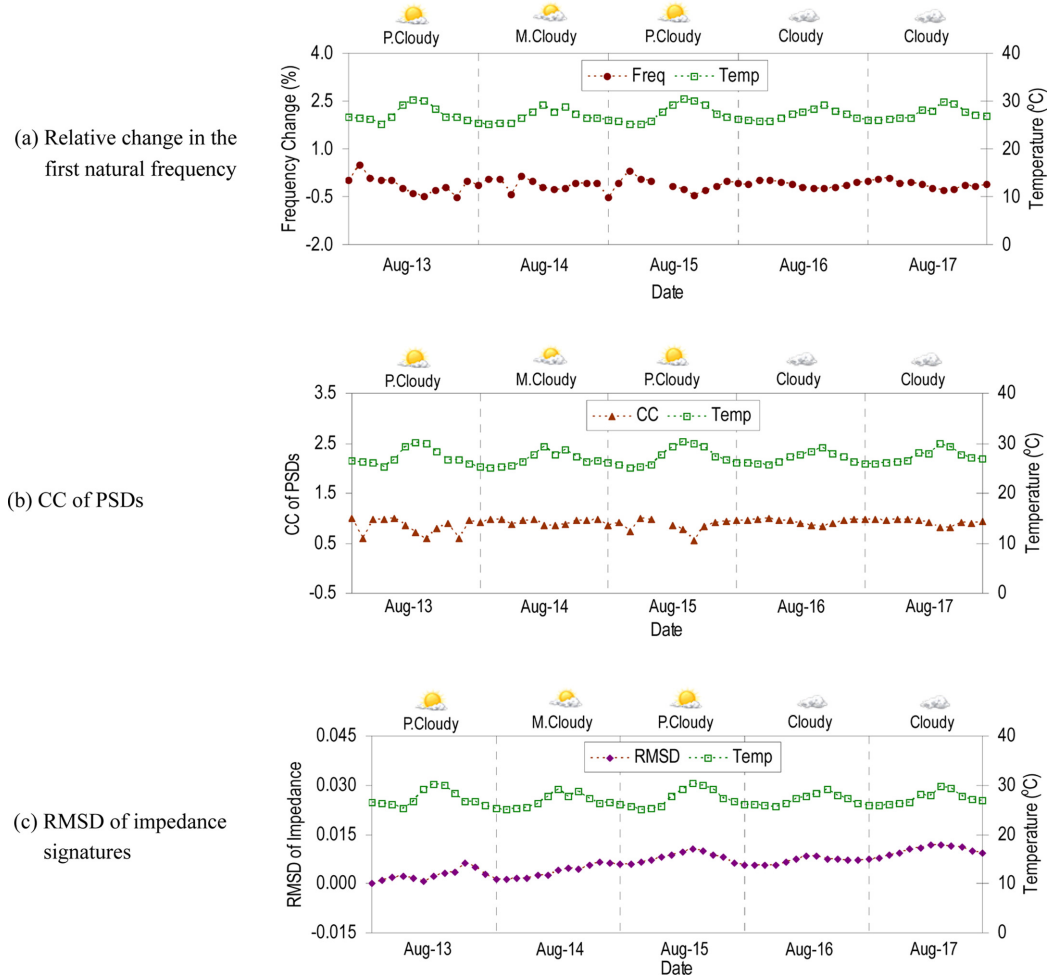
Fig. 14 Vibration and impedance monitoring under various temperatures for cable C3

Table 2 Structural properties, natural frequencies, and estimated forces of cables C1~C5

Cable	Anchorage type	Span length (m)	Designed force (kN)	Parameter ξ	Theoretical freqs. (Hz)			Experimental freqs. (Hz)			Estimated force (kN)	
					Mode 1	Mode 2	Mode 3	Mode 1	Mode 2	Mode 3		
C1	73H	123.806	7456.3	247.8	1.097	2.195	3.292	1.139	2.270	3.404	7857.8	(5.4)
C2	55H	72.733	4728.4	153.9	1.711	3.422	5.133	1.741	3.452	5.143	4681.1	(1.0)
C3	49H	44.893	4828.0	107.7	2.978	5.956	8.933	2.912	5.668	8.702	4332.3	(10.3)
C4	55H	78.364	4278.9	157.7	1.511	3.021	4.532	1.559	3.107	4.619	4386.8	(2.5)
C5	85H	136.813	9612.4	267.1	1.042	2.083	3.125	1.053	2.104	3.155	9652.1	(0.4)

*Parentheses indicate differences (%) of estimated forces with respect to designed forces

4.3.2 Long-term cable force monitoring

For long-term monitoring of cable force, cable C5 was selected as the target cable. Table 3 shows the change in natural frequencies, cable force of cable C5 due to the temperature variation. It is found that the natural frequencies tend to decrease with the increment of temperature. The change in
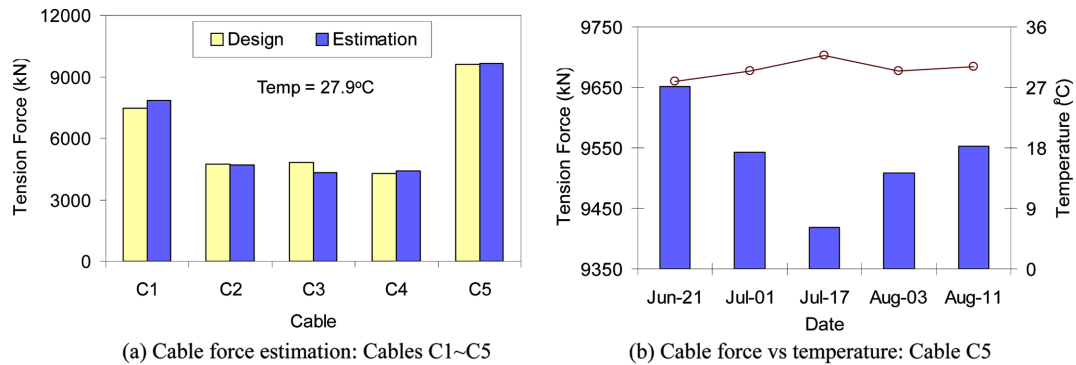
(a) Cable force estimation: Cables C1~C5   (b) Cable force vs temperature: Cable C5

Fig. 15 Cable force estimation and monitoring

Table 3 Experimental natural frequencies, and cable force of cable C5 vs temperature

Date		Jun-21	Jul-01	Jul-17	Aug-03	Aug-11
Temperature (^{o}C)		27.9	29.4	31.8	29.4	30.1
Experimental frequencies (Hz)	Mode 1	1.053	1.048	1.032	1.044	1.048
	Mode 2	2.104	2.094	2.090	2.092	2.096
	Mode 3	3.155	3.132	3.127	3.132	3.137
Cable force (kN)		9652.1	9542.6	9419.1	9507.9	9553.5

cable force due to the temperature change is also investigated. Fig. 15(b) shows the cable forces which are estimated at various temperatures during the monitoring period. As shown in Fig. 15(b) and also listed in Table 3, it is observed that the cable force tends to decrease as the temperature goes up, and vice versa. This issue can be explained by the relaxation of cable due to the temperature increment.

4.4 Experimental modal identification of test bridge

4.4.1 Numerical modal analysis

In order to analyze numerical modal parameters and to identify the corresponding experimental modal parameters of the test bridge, a finite element (FE) model of Hwamyung Bridge was established using SAP2000 as shown in Fig. 16. Two pylons and main girder were modeled by frame elements with dimensions as same as bridge design drawing. Stayed-cables were modeled by cable elements with equivalent circular cross sections which have the same total areas with designed ones. By modeling as cable element, nonlinear stiffness of cable due to post tension force was taken into account. Material properties of girder and two pylons were defined as concrete with Young's modulus of 28.6 GPa, Poisson's ratio of 0.2, and mass density of 2500 kg/m³. Meanwhile, material properties of cables were defined as steel with Young's modulus of 195 GPa, Poisson's ratio of 0.3, and mass density of 7850 kg/m³. Two pylons were assumed totally fixed at the bottom. Two girder ends were supported by rollers in vertical direction and by springs in horizontal direction. Modal parameters of the FE model were analyzed with consideration of p-delta effects of cable post tensions.

4.4.2 Experimental modal identification

In order to extract experimental natural frequencies and mode shapes of deck and pylon, the SSI method (Yi and Yun 2004) was performed. Fig. 17 shows the stabilization chart obtained in the SSI
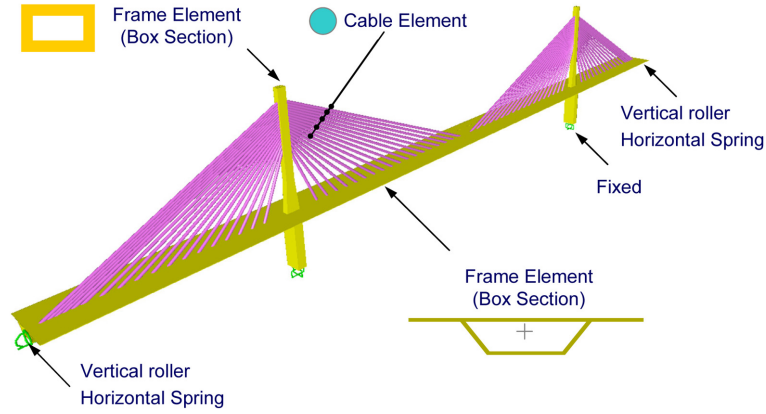
Fig. 16 FE model of Hwamyung Bridge

process for vertical and transverse responses. The first six vertical bending modes (i.e., V1~V6) and three transverse bending modes (i.e., L1~L3) were extracted. The corresponding mode shapes and natural frequencies are given in Fig. 18 and also listed in Table 4. As shown in Fig. 18, the mode shapes of bridge were well extracted by the six Imote2/SHM-H sensor nodes on deck and pylon (i.e., five locations on deck and one location on top pylon). Also, the numerical modal analyses show good agreement with experimental results. The differences of natural frequency range from 0.4% to 9.6%. Those differences are moderate for the initial FE model based on the design parameters. In future study, the FE model should be fine-tuned appropriately to represent the behaviors of the bridge.

5. Conclusions

In this paper, the feasibility of solar-powered, multi-scale, vibration-impedance sensor node on Imote2 platform was successful evaluated for hybrid SHM in a full-scale cable-stayed bridge. First, vibration- and impedance-based hybrid SHM methods were briefly outlined. Second, the multi-scale sensor node was described on the design of hardware components and embedded software for vibration- and impedance-based SHM. In this approach, a solar-powered energy harvesting was
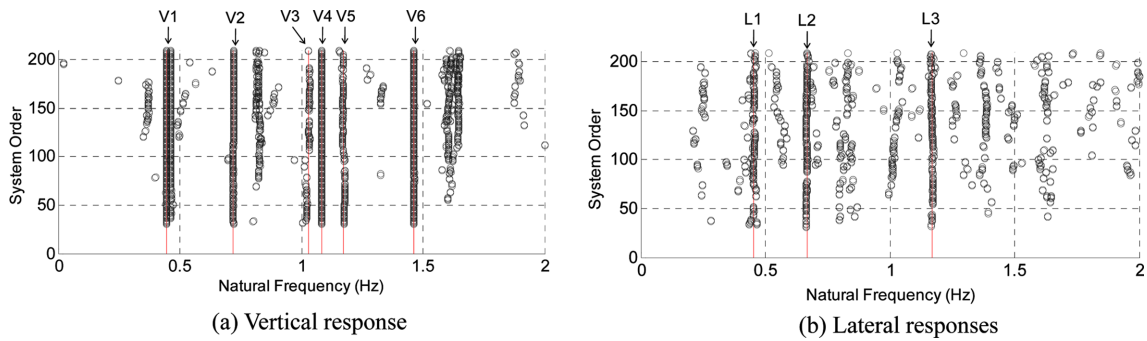

(a) Vertical response   (b) Lateral responses

Fig. 17 SSI method: Stabilization charts

Table 4 Numerical and experimental natural frequencies (Hz) of deck and pylon

	Vertical modes						Lateral modes		
	V1	V2	V3	V4	V5	V6	L1	L2	L3
FE model	0.468	0.686	1.098	1.17	1.296	1.57	0.443	0.669	1.142
Experiment	0.444	0.72	1.028	1.084	1.171	1.462	0.454	0.666	1.169
Difference (%)	5.1	5.0	6.4	7.4	9.6	6.9	2.5	0.4	2.4

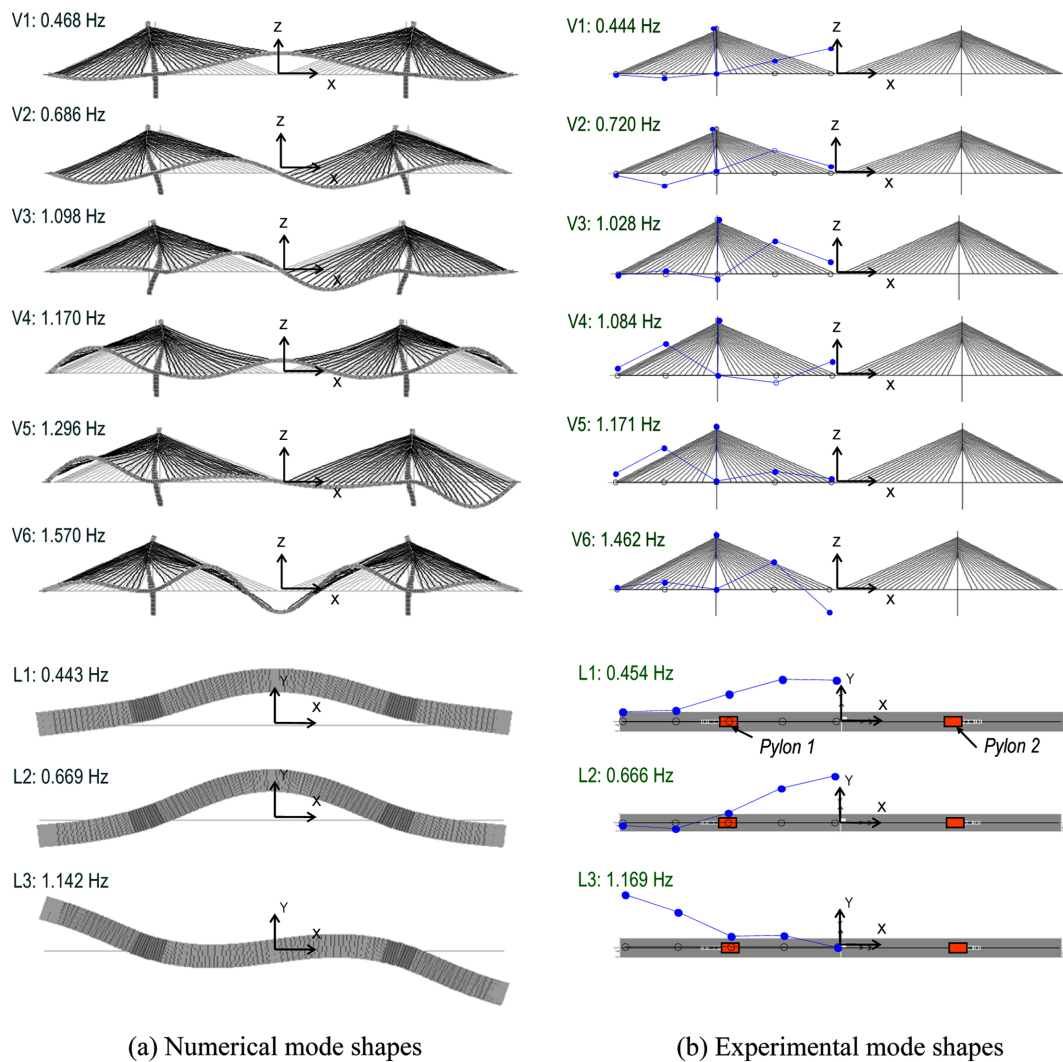(a) Numerical mode shapes   (b) Experimental mode shapes

Fig. 18 Modal identification for deck and pylon

implemented for autonomous operation of the smart sensor node. Finally, the performance of smart sensor nodes was successful evaluated on Hwamyung cable-stayed bridge in Korea.

The sensor nodes were well responsive up to 90% successful level for wireless communication. The charging process of solar-harvesting system designed for smart sensor nodes worked stably for long-term monitoring. Vibration responses under typhoon condition were measured and analyzed in

comparison with those under normal condition. Also, vibration and impedance responses measured from the target bridge were examined for the robust long-term monitoring capability of the smart sensor system. Cable force was successfully monitored by acceleration sensor nodes with consideration of temperature variation. Modal parameters (i.e., natural frequencies and mode shapes) were also accurately extracted by the smart sensor nodes. The success of field experiment on Hwamyung Bridge demonstrates the potential of smart sensor techniques for hybrid SHM in civil infrastructures. Future works will focus on developing hybrid SHM software for autonomous long-term monitoring of bridge.

Acknowledgements

References

Adams, R.D., Cawley, P., Pye, C.J. and Stone, B.J. (1978), "A vibration technique for nondestructive assessing the integrity of structures", *J. Mech. Eng. Sci.*, **20**(2), 93-100.

Analog Devices (2010), "Datasheet of AD5933", Available at http://www.analog.com.

Brincker, R., Zhang. L. and Andersen, P. (2001), "Modal identification of output-only using frequency domain decomposition", *Smart Mater. Struct.*, **10**(3), 441-445.

Cho, S., Jo, H., Jang, S., Park, J., Jung, H.J., Yun, C.B., Spencer, Jr, B.F. and Seo., J.W. (2010), "Structural health monitoring of a cable-stayed bridge using smart sensor technology: data analyses", *Smart Struct. Syst.*, **6**(5-6), 461-480.

Clough, R.W. and Penzien, J. (1993), *Dynamics of structures*, 2nd Ed., McGraw-Hill.

Crossbow Technology (2007), "Imote2 hardware reference manual, revision A", Available at http://www.xbow.com.

Doebling, S.W., Farrar, C.R. and Prime, M.B. (1998), "A summary review of vibration-based damage identification methods", *Shock Vib.*, **30**(2), 91-105.

Farrar, C.R. (2001), *Historical overview of structural health monitoring*, Lecture Notes on Structural Health Monitoring Using Statistical Pattern Recognition, Los Alamos Dynamics, Los Alamos, NM.

Illinois Structural Health Monitoring Project (2011), *Imote2 for Structural Health Monitoring: User's Guide*, University of Illinois at Urbana-Champaign.

Jang, S., Jo, H., Cho, S., Mechitov, K., Rice, J.A., Sim, S.H., Jung, H.J., Yun, C.B., Spencer, Jr, B.F. and Agha, G. (2010), "Structural health monitoring of a cable-stayed bridge using smart sensor technology: deployment and evaluation", *Smart Struct. Syst.*, **6**(5-6), 439-459.

Jo, H., Rice, J.A., Spencer, B.F. and Nagayama, T. (2010), "Development of a high-sensitivity accelerometer board for structural health monitoring", *Proceedings of the SPIE*, San Diego, USA.

Kim, J.T., Park, J.H. and Lee, B.J. (2006), "Vibration-based damage monitoring in model plate-girder bridges under uncertain temperature conditions", *Eng. Struct.*, **29**(7), 1354-1365.

Kim, J.T., Park, J.H., Hong, D.S. and Ho, D.D. (2011), "Hybrid acceleration-impedance sensor nodes on Imote2-platform for damage monitoring in steel girder connections", *Smart Struct. Syst.*, **7**(5), 393-416.

Kim, J.T., Park, J.H., Hong, D.S. and Park, W.S. (2010), "Hybrid health monitoring of prestressed concrete girder bridges by sequential vibration-impedance approaches", *Eng. Struct.*, **32**(1), 115-128.

Koo, K.Y. (2008), *Structural health monitoring methods for bridges using ambient vibration and impedance measurements*, Doctoral Dissertation, Korea Advanced Institute of Science and Technology, Deajeon. Korea.

Liang, C., Sun, F.P. and Rogers, C.A. (1996), "Electro-mechanical impedance modeling of active material systems", *Smart Mater. Struct.*, **5**(2), 171-186.

Lynch, J.P., Wang, W., Loh, K.J., Yi, J.H. and Yun, C.B. (2006), "Performance monitoring of the Geumdang bridge using a dense network of high-resolution wireless sensors", *Smart Mater. Struct.*, **15**(6), 1561-1575.

Mascarenas, D.L., Todd, M.D., Park, G., and Farrar, C.R., (2007), "Development of an impedance-based wireless sensor node for structural health monitoring", *Smart Mater. Struct.*, **16**(6), 2137-2145.

Memsic Co. (2010), "Datasheet of ISM400", Available at http://www.memsic.com.

Miller, T.I., Spencer, B.F., Li, J. and Jo, H. (2010), *Solar energy harvesting and software enhancements for autonomous wireless smart sensor networks*, NSEL Report Series, NSEL-022.

Nagayama, T., Spencer, B.F. and Rice, J.A. (2009), "Autonomous decentralized structural health monitoring using smart sensors", *Struct. Health Monit.*, **16**, 842-859.

Park, G., Kabeya, K., Cudney., H.H. and Inman, D.J. (1999), "Impedance-based structural health monitoring for temperature varying applications", *JSME Int. J. A-Solid M.*, **42**(2), 249-258.

Park, G., Sohn, H., Farrar, C. and Inman, D. (2003), "Overview of piezoelectric impedance-based health monitoring and path forward", *Shock Vib.*, **35**, 451-463.

Park, J.H., Kim, J.T., Hong, D.S., Mascarenas, D. and Lynch, J.P. (2010), "Autonomous smart sensor nodes for global and local damage detection of prestressed concrete bridges based on accelerations and impedance measurements", *Smart Struct. Syst.*, **6**(5-6), 711-730.

Raghavan, A. and Cesnik, E.S. (2007), "Review of guided-wave structural health monitoring", *Shock Vib.*, **39**(2), 91-114.

Rice, J.A., Mechitov, K., Sim, S.H., Nagayama, T., Jang, S., Kim, R., Spencer, Jr, B.F., Agha, G. and Fujino, Y. (2010), "Flexible smart sensor framework for autonomous structural health monitoring", *Smart Struct. Syst.*, **6**(5-6), 423-438.

Shimada, T. (1995), *A study on the maintenance and management of the tension measurement for the cable of bridge*, Ph.D. Dissertation, Kobe University, Japan.

Sohn, H., Farrar, C.R., Hemez, F.M., Shunk, D.D., Stinemates, D.W. and Nadler, B.R. (2003*), A review of structural health monitoring literature: 1996-2001*, Los Alamos National Laboratory Report, LA-13976-MS, Los Alamos, NM.

Spencer, B.F. and Cho, S. (2011), "Wireless smart sensor technology for monitoring civil infrastructure: Technological developments and full-scale applications", *Proceeding of the World Congress on Advances in Structural Engineering and Mechanics (ASEM'11 Plus)*, Seoul, Korea.

Spencer, B.F., Ruiz-Sandoval, M.E. and Kurata, N. (2004), "Smart sensing technology: opportunities and challenges", *Struct. Health Monit.*, **11**(4), 349-368.

Straser, E.G. and Kiremidjian, A.S. (1998), *A modular, wireless damage monitoring system for structure*, Technical Report 128, John A. Blume Earthquake Engineering Center, Stanford University, Stanford, CA.

Stubbs, N. and Kim, J.T. (1996), "Damage localization in structures without baseline modal parameters", *AIAA J.*, **34**(8), 1644-1649.

Sun, F.P., Chaudhry, Z., Rogers, C.A. and Majmundar, M. (1995), "Automated real-time structure health monitoring via signature pattern recognition", *Proceedings of the SPIE*, San Diego, USA.

Yi, J.H. and Yun, C.B. (2004), "Comparative study on modal identification methods uing output-only information", Struct. Eng. Mech., **17**(7), 927-944.

Zui, H., Shinke, T. and Namita, Y. (1996), "Practical formulas for estimation of cable tension by vibration method", *J. Struct. Eng - ASCE*, **122**(6), 651-656.

CC